Nonequilibrium dynamics of the Holstein polaron driven by an external electric field

Lev Vidmar,[1] Janez Bonča,[1,2] Marcin Mierzejewski,[1,3] Peter Prelovšek,[1,2] and Stuart A. Trugman[4]
[1]*J. Stefan Institute, 1000 Ljubljana, Slovenia*
[2]*Faculty of Mathematics and Physics, University of Ljubljana, 1000 Ljubljana, Slovenia*
[3]*Institute of Physics, University of Silesia, 40-007 Katowice, Poland*
[4]*Theoretical Division, Los Alamos National Laboratory, Los Alamos, New Mexico 87545, USA*
(Received 8 January 2011; revised manuscript received 11 February 2011; published 5 April 2011)

This work represents a fundamental study of a Holstein polaron in one dimension driven away from the ground state by a constant electric field. Taking fully into account quantum effects, we follow the time evolution of the system from its ground state as the constant electric field is switched on at $t = 0$ until it reaches a steady state. At weak electron-phonon coupling (EP), the system experiences damped Bloch oscillations (BO's) characteristic for a noninteracting electron band. An analytic expression of the steady-state current is proposed in terms of weak EP coupling and large electric field. For moderate values of EP coupling, the oscillations are almost critically damped and the system reaches the steady state after a short time. In the strong-coupling limit, weakly damped BO's, consistent with nearly adiabatic evolution within the polaron band, persist up to extremely large electric fields. A traveling polaron under the influence of the electric field leaves behind a trail of phonon excitations absorbing the excess energy gained from the electric field. The shape of the traveling polaron is investigated in detail.

DOI: 10.1103/PhysRevB.83.134301 PACS number(s): 71.38.−k, 63.20.kd, 72.10.Di, 72.20.Ht

I. INTRODUCTION

Research in the field of nonequilibrium dynamics of complex quantum systems constitutes a formidable theoretical challenge. Many advanced numerical techniques, including exact diagonalization,[1] expansion using Chebyshev polynomials,[2] time-dependent density-matrix renormalization group,[3] and nonequilibrium dynamical mean-field techniques,[4] have been developed to tackle this complex problem.

More than 40 years ago, using a path-integral approach, Thornber and Feynman[5] discovered that an electron in a parabolic band, driven by the electric field, acquires a constant velocity due to the emission of phonons. Later approaches to polaron motion in high electric field used Boltzmann equations,[6] and the high-field drift velocity was estimated via phonon-assisted hopping between different rungs of Wannier-Stark states using rate equations.[7,8] In Ref. 9, the one-dimensional Holstein polaron problem in a strong electric field was mapped on a nonstandard Bethe lattice. It was realized that keeping full quantum coherence between many-body states is crucial to obtain finite drift velocity for dispersionless optical phonons. Extensive research of polaron dynamics has been conducted within the semiclassical Su-Shrieffer-Heeger model to describe the properties of conjugated polymers that may be used in a variety of applications such as molecular electronics or light-emitting diodes.[10–15] Polaron formation and its influence on transport properties have also been investigated in the context of DNA molecules within the semiclassical Peyrard-Bishop-Holstein model[16–22] and other polaronlike models.[23–25]

Bloch oscillations (BO's) represent a fundamental phenomenon in quantum mechanics where a charged particle in a periodic potential exhibits a periodic motion when exposed to a uniform external electric field. Since the electrons in solids can dissipate energy due to scattering from inelastic degrees of freedom on a time scale usually shorter than a typical Bloch time t_B, it took a long time until the first experimental observation of BO's was carried out on semiconducting superlattices[26–30] and later in optical potentials.[31–33] Nowadays, the concept of BO's is frequently present in a variety of different fields, for instance atomic Bose-Einstein condensates in optical lattices,[34–37] interacting quantum few-body systems,[38–40] or organic molecules.[14,21,22,41] However, the description of the damping of BO's in a dissipative medium remains a challenging task.

By choosing the Holstein Hamiltonian as one of the simplest model systems describing the interaction between a fermion and phonons, we are able to investigate the field-induced acceleration of the polaron, which simultaneously dissipates the energy by inelastic scattering on optical phonons while maintaining the full quantum nature of the problem. Following the time evolution of the ground state when the electric field is switched on at time $t = 0$, we show how the polaron reaches the steady state and consequently develops a constant nonzero velocity. In particular, we calculate the steady-state current versus voltage characteristics of the Holstein polaron for different regimes of electron-phonon couplings.

We discuss the Holstein model in one spacial dimension and give a brief overview of the numerical method in the second section. In the third section, we discuss numerical results. Here we give special emphasis on the time evolution from the ground state toward the steady state by presenting various correlation functions in different electron-phonon (EP) coupling regimes. We compare our results with a simple Landau-Zener model and follow the time evolution of the polaron as it starts propagating after switching on the electric field. As a focal point of this work, we discuss the dependence of the steady-state current on the EP coupling and electric field. In the final section we present the conclusions.

II. MODEL AND NUMERICAL METHOD

We analyze the one-dimensional Holstein model with a single electron, threaded by a time-dependent flux:

$$H = -t_0 \sum_i (e^{i\theta(t)} c_i^\dagger c_{i+1} + \text{H.c.}) + g \sum_i n_i (a_i^\dagger + a_i) + \omega_0 \sum_i a_i^\dagger a_i, \quad (1)$$

where $c_i^\dagger$ and $a_i^\dagger$ are electron and phonon creation operators at site i, respectively, and $n_i = c_i^\dagger c_i$ is the electron density. ω_0 denotes a dispersionless optical phonon frequency and t_0 is the nearest-neighbor hopping amplitude. The dimensionless EP coupling strength is $\lambda = g^2/2t_0\omega_0$. The constant electric field F that is switched on at time $t = 0$ enters the Hamiltonian in Eq. (1) through the time-dependent phase $\theta(t) = -Ft$ for $t \geqslant 0$. We measure the electric field F in units of $[t_0/e_0 a]$, where e_0 is the unit charge and a is the lattice distance. We furthermore measure time in units of $[\hbar/t_0]$. Unless otherwise specified, from here on we set $a = e_0 = \hbar = t_0 = 1$.

To solve the time-dependent Hamiltonian for a single electron coupled to phonon degrees of freedom, we use an improved numerical method, originally introduced in Ref. 42, that led to numerically exact solutions of the polaron ground and low-lying excited-state properties. The method constructs the variational Hilbert space (VHS) starting from the single-electron Bloch state $c_{\mathbf{k}}^\dagger|\emptyset\rangle$ with no phonons on an infinite lattice. The VHS is then generated by applying the off-diagonal terms of Hamiltonian (1),

$$\{|\phi_{\mathbf{k},l}^{(N_h,M)}\rangle\} = \left(H_{\text{kin}} + H_{\text{g}}^M\right)^{N_h} c_{\mathbf{k}}^\dagger|\emptyset\rangle, \quad (2)$$

where H_{kin} and H_{g} correspond to the first and the second term of the Hamiltonian in Eq. (1), respectively. Parameters N_h and M determine the size of the VHS. In addition, $N_h - 1$ represents the maximum distance between the electron and the phonon quanta and $N_h * M$ is the maximum number of phonon quanta contained in the Hilbert space. The parameter $M > 1$ (Ref. 43) ensures good convergence in the strong EP coupling regime that contains multiple phonon excitations. To reach the weak-coupling regime, $\lambda \ll 1$, we introduce an additional parameter N_{phmax} limiting the maximum total number of phonon quanta, which enables construction of VHS as large as $N_h = 40$.

We first solve the Hamiltonian in Eq. (1) for $F = 0$, i.e., we calculate the (zero-temperature) polaron ground state.[42,44–53] Then we switch on the uniform electric field and start the time propagation from the initial state using the time-dependent Lanczos technique.[54] We manage to find numerically accurate results of the model away from equilibrium while maintaining a full quantum description of phonons. Since we are dealing with a single particle in an infinite system, we compute the time-dependent average of the current operator $j(t) = \langle \hat{I}(t) \rangle$, where

$$\hat{I}(t) = i\left(\sum_l e^{-iFt} c_l^\dagger c_{l+1} - \text{H.c.}\right). \quad (3)$$

In the case of a time-independent field F, the time integral of the current is directly related to a change of the total energy,

$$\int_0^t j(t')dt' = \Delta h(t)/F = x(t), \quad (4)$$

where $\Delta h(t) = \langle H(t) \rangle - \langle H(t=0) \rangle$ and $x(t)$ represents the traveled distance.[55]

III. NUMERICAL RESULTS

A. Time evolution from the ground state toward the steady state

We first present results obtained near the noninteracting limit, i.e., at $\lambda = 0.01$, where $j(t)$ displays damped BO's around $j(t \to \infty) > 0$, see Fig. 1(a). The period and the initial amplitude of BO's at small t are consistent with BO's of a free electron, denoted with a thin dashed line in Fig. 1(a). Damping is due to inelastic scattering on phonons that is in turn reflected in a monotonic increase of the average phonon number $\langle n_{\text{ph}} \rangle$ with time, as depicted in Fig. 1(c). Damping is, however, not the most important consequence of inelastic scattering. Notably, $j(t)$ approaches a positive steady-state current $\bar{j}$ for $t > t_s \sim 4t_B$ and $6t_B$ at $F = 1/5$ and $1/2$, respectively, where t_B denotes the Bloch oscillation period $t_B = 2\pi/F$. Note that $\bar{j} \ll j_{\max} = 2$. The dependence of the steady-state current $\bar{j}$

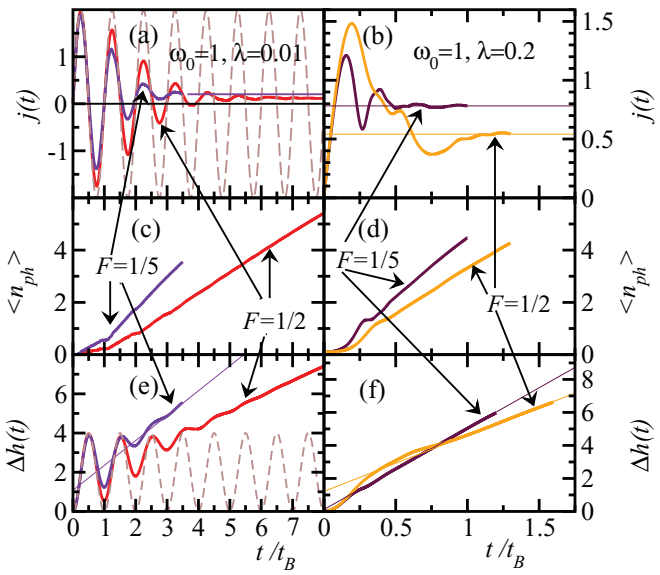

FIG. 1. (Color online) $j(t)$ vs t/t_B for two values of $F = 1/5$ and $1/2$ for $\omega_0 = 1$, and two distinct values of λ: (a) $\lambda = 0.01$ and (b) $\lambda = 0.2$. Thin dashed line in (a) represents $j(t)$ for $\lambda = 0$, thin horizontal lines in (a) and (b) indicate steady-state values $\bar{j}$; $\langle n_{\text{ph}} \rangle$ is shown in (c) and (d) for the same set of parameters as in (a) and (b), respectively; corresponding averages $\Delta h(t)$ are displayed in (e) and (f). Thin dashed line in (e) represents $\Delta h(t)$ for $\lambda = 0$. The accuracy of time propagation was checked by comparison of the energy-gain sum rule, Eq. (4). Parameters defining the functional generator [Eq. (2)] were $N_h = 40$, $M = 1$, and $N_{\text{phmax}} = 6$ for $F = 1/5$; and $N_h = 28$, $M = 1$, and $N_{\text{phmax}} = 8$ for $F = 1/2$. In this and all subsequent figures, we used up to $N_{\text{st}} \sim 15 \times 10^6$ states in the Hilbert space and $N_{\text{step}} = 2000$ time steps within each t_B. Different sizes of VHS were used to check the convergence in the thermodynamic limit. Thin straight lines represent $t \to \infty$ extrapolations.

on F will be discussed further in the text. The steady-state current as well emerges as a linear dependence of the total energy on time: $\Delta h(t) = F\bar{j}t + \Delta h_0$, see results in Fig. 1(e), where with increasing t, $\Delta h(t)$ approaches a straight line. In the steady state, we also observe a linear increase of $\langle n_{\rm ph}\rangle$ versus t. When comparing $\Delta h(t)$ and $\langle n_{\rm ph}\rangle$ in the linear regime, we find that $\Delta\dot{h}(t) = \omega_0 {\rm d}\langle n_{\rm ph}\rangle/{\rm d}t$. This equality confirms an intuitive expectation that in the steady state, the total energy gain is entirely absorbed by the lattice.

On a more technical note, we note that to reach a steady state, the Hilbert space used in our calculation must contain a large enough set of excited states that in turn represent the reservoir for the absorption of energy. For this reason, different Hilbert spaces were used, depending on the strength of EP coupling and the size of F; see also the caption of Fig. 1.

At a larger value of EP coupling, $\lambda = 0.2$, a somewhat different physical picture emerges, as shown in Figs. 1(b), 1(d), and 1(f). The main differences can be summarized as follows: (i) BO's become overdamped, (ii) $j(t)$ remains positive at all t, and (iii) $j(t)$ reaches a steady state after a short time $t_s \lesssim t_B$. Characteristic for a steady state are linear t dependencies of $\langle n_{\rm ph}\rangle$ and $\Delta h(t)$ in Figs. 1(d) and 1(f), respectively. Common to all cases presented in Fig. 1 is the emergence of a constant steady-state current for $t > t_s$.

In Figs. 2(a) and 2(b), we present current versus time in the strong-coupling regime, i.e., at $\lambda = 2.0$. At $F = 1/10$ [Fig. 2(a)], we observe nearly undamped BO's as the polaron adiabatically follows the polaron band. Regular oscillations in $\langle n_{\rm ph}\rangle$ and $\Delta h(t)$ in Figs. 2(c) and 2(e) portray polaron averages nearly identical to their ground-state values at corresponding wave vectors $k = Ft = 2\pi t/t_B$. The response of the system to external field is nearly elastic, since $\Delta h(t = l * t_B) \sim 0$

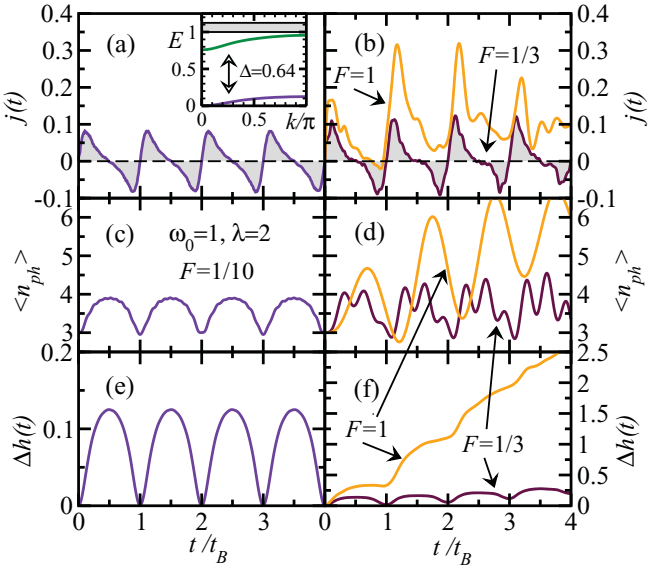

FIG. 2. (Color online) $j(t)$ in (a) and (b), $\langle n_{\rm ph}\rangle$ in (c) and (d), and $\Delta h(t)$ in (e) and (f) vs t/t_B for $\omega_0 = 1$ and $\lambda = 2$ and three different values of F as indicated in the figures. Inset in (a) shows the polaron spectrum (ground state, first excited state energy, and the continuum vs the wave vector k) for $\omega_0 = 1$ and $\lambda = 2$. Note that there is a different vertical scale used in (e) and (f). We used $N_h = N_{\rm phmax} = 20$ and $M = 1$ with $N_{\rm st} = 3 \times 10^6$.

for any integer value of l. The average current remains indistinguishable from zero in the largest time interval tested with our calculation, i.e., $t \leqslant 20t_B$.

To illuminate this behavior, we note that in the strong-coupling limit a large gap Δ exists in the polaron excitation spectrum being of the order of ω_0. The low-energy polaron excitation spectrum is presented for $\omega_0 = 1$ and $\lambda = 2$ in the inset of Fig. 2(a), where a gap $\Delta \sim 0.64$ separates the polaron band from the excited polaron band,[42,56–58] located just below the continuum denoted by the gray area. At small $F \ll \Delta$, there exists an exponentially small probability for a nonadiabatic transition from the polaron band to the excited polaron band or/and into the continuum.

For sufficiently large F [see Figs. 2(b), 2(d), and 2(f)] for $F = 1/3$ and 1, BO's in $j(t)$ lose periodicity even though remnants of BO's remain clearly visible, and the time-averaged current becomes finite (nonzero). Additional frequencies appear in $\langle n_{\rm ph}\rangle$ that indicate multiple phonon excitations due to polaron transitions to excited polaron bands. Moreover, the average value of $\langle n_{\rm ph}\rangle$ between successive t_B intervals increases. The total energy $\Delta h(t)$ also increases in time. At large field, $F = 1$, $\Delta h(t)$ approaches a straight line signaling the onset of a steady state.

B. Determination of the threshold electric field using the Landau-Zener formalism

The observed behavior in the strong-coupling regime due to a large gap in the spectrum resembles the Landau-Zener (LZ) transition,[59,60] where the probability for tunneling between bands in a two-level system,

$$H(t) = \begin{pmatrix} vFt & \Delta/2 \\ \Delta/2 & -vFt \end{pmatrix}, \tag{5}$$

is given by

$$P = \exp\left[-\pi \frac{(\Delta/2)^2}{vF}\right], \tag{6}$$

where Δ is the energy gap between the two levels and v is the velocity. Using Eq. (6), we estimate the threshold electric field $F_{\rm th}$ using

$$F_{\rm th} = \frac{(\Delta/2)^2}{v}. \tag{7}$$

Such an estimate has been used to determine the dielectric breakdown of the insulating half-filled Hubbard model.[1,61] Applying Eq. (7) to the specific case of $\lambda = 2$ presented in Fig. 2, using $\Delta \sim 0.64$ and $v = j_{\rm max} \sim 0.1$, we obtain $F_{\rm th} \sim 1.0$. The LZ formalism gives roughly the correct order of magnitude of $F_{\rm th}$, since a noticeable current appears around $F = 1/3$, as seen in Figs. 2(b) and 2(f), as well as from steady-state current presented in Fig. 4(c). One should, however, be mindful when considering the LZ formalism. In the polaron case, the band structure deviates significantly from the ideal LZ model with two hyperbolic bands. In the realistic case, multiple transitions occur from the polaron band to a continuum of excited states composed of a polaron and additional phonon degrees of freedom.

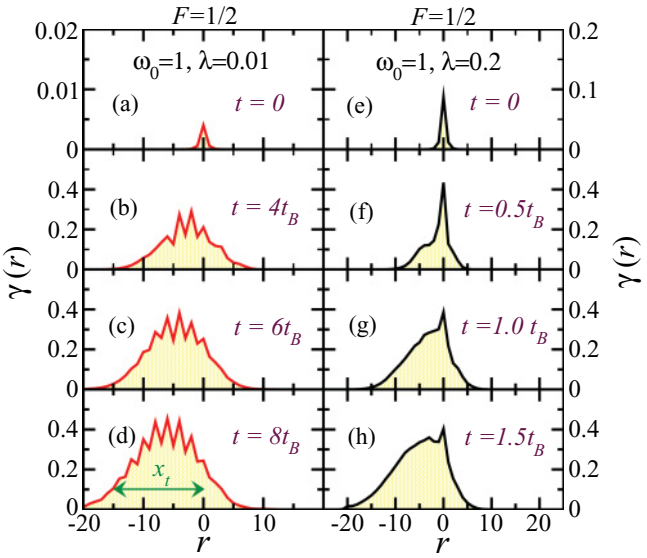

FIG. 3. (Color online) $\gamma(r)$ for $\omega_0 = 1$, $\lambda = 0.01$, and $F = 1/2$ in (a)–(d) and $\lambda = 0.2$ in (e)–(h) computed at different times. The electric field is switched on at $t = 0$. Note a vertical scale change between (a) and (b) as well as between (e) and (f). x_t in (d) represents the traveled distance; see discussion in the text.

C. Time evolution of the polaron

In Fig. 3, we follow the time evolution of the polaron toward steady state at $F = 1/2$. We compute the average number of phonon quanta located at a given distance r from the electron,

$$\gamma(r) = \left\langle \sum_i n_i a^+_{i+r} a_{i+r} \right\rangle, \tag{8}$$

fulfilling the sum rule $\langle n_{\rm ph}\rangle = \sum_r \gamma(r)$. At $t = 0$, $\gamma(r)$ displays a pronounced peak at the position of the electron, i.e., at $r = 0$, consistent with the shape of the polaron in its $k = 0$ ground state. After the electric field is switched on, $\gamma(r)$ experiences a compelling time evolution with three outstanding characteristics: (i) the overall increase of $\gamma(r)$ with time, (ii) the development of pronounced asymmetry of $\gamma(r)$ with respect to the electron position at $r = 0$, and (iii) an increased amount of polaron excitations in the forward direction. The overall increase of $\gamma(r)$ is consistent with the absorption of energy that is deposited in an increasing number of phonon excitations. The asymmetry is a result of a growing phonon tail, extending behind the moving polaron. Note that the polaron is moving from left to right. In the long time limit, γ is expected to be approximately constant, independent of r and t, for r sufficiently negative. The average height of the polaron tail $\bar\gamma$ is due to the energy conservation requirement independent of λ:

$$x(t)F \sim \langle n_{\rm ph}\rangle\omega_0 \sim x(t)\bar\gamma\omega_0, \tag{9}$$

therefore $\bar\gamma \sim F/\omega_0$; compare Figs. 3(d) and 3(h). Note that this relation holds only when the system has reached a steady state. The length of the polaron tail is given by the expression for the traveled distance $x(t) = \Delta h(t)/F$. At $t = 8t_B$ and $\lambda = 0.01$, we obtain from Fig. 1(e) $x_t = x(8t_B) \sim 14.8$, which fits well with the length of the phonon tail in Fig. 3(d).

Rather unexpected is the pronounced increase of phonon excitations in the forward direction where $\gamma(r) \gtrsim 0$ up to $r \leqslant r_f \sim 5 - 7$ for all $t > 0$ presented in Fig. 3. Since time evolution starts from the ground state at zero temperature, there are no phonon excitations present far ahead of the moving electron. A substantial forward tail of phonon excitations is a consequence of damped BO's. Indeed, r_f compares well with the Stark localization length, i.e., $r_f \sim L_S = 4/F = 8$. Yet another intriguing feature in $\gamma(r)$ emerges as regular oscillations in the polaron tail with a period $K = \omega_0/F = 2$, clearly seen in the small $\lambda = 0.01$ limit; see Figs. 3(b)–3(d). At larger $\lambda = 0.2$, these oscillations become overdamped.

D. Steady-state current

The focal point of this work is the calculation of the steady-state current $\bar j$ and analysis of its dependence on F and λ. In Fig. 4, we present the current-voltage characteristics, i.e., $\bar j$ versus F for different values of λ. Note that the upper limit of $\bar j$ is given by the current amplitude $j_{\rm max} = 2$ in the noninteracting system. We have limited our calculations to commensurate values $F = \omega_0/K$ (where K is an integer) with two exceptions: (i) large $F > \omega_0$, where we have chosen $F = 2\omega_0, 3\omega_0, \ldots$, and (ii) results presented with disconnected

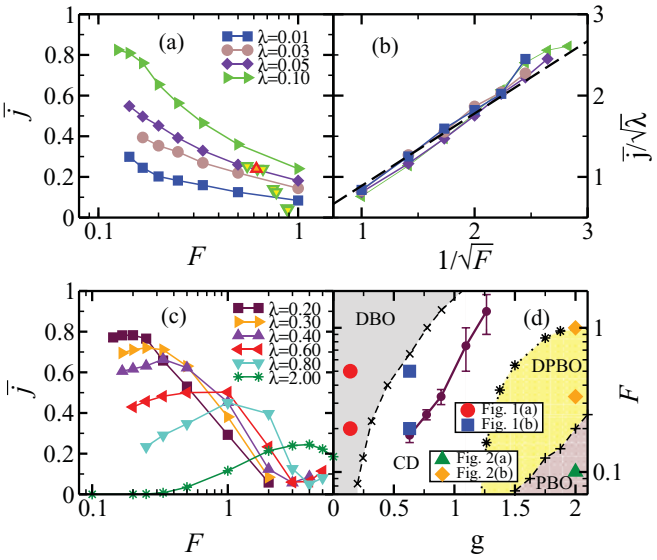

FIG. 4. (Color online) Steady-state current $\bar j$ vs F in the weak-coupling limit in (a) and in the weak- to intermediate-coupling regime in (c), scaling $\bar j/\sqrt{\lambda}$ vs $1/\sqrt{F}$ in the weak-coupling limit in (b), and diagram, presenting different regimes, as described in the text (d). Also in (d), circles with error bars indicate positions in the diagram where for a fixed g, a maximum value $\bar j_{\rm max}$ was reached; isolated circles, squares, and diamonds indicate values used for Figs. 1 and 2. Disconnected triangles (seven down and one up) in (a) represent $\bar j$ using noninteger values (seven rational and one irrational) of $1/F$, i.e., $F = 5/9, 2/(1+\sqrt{5}), 5/8, 6/9, 6/8, 7/9, 7/8$, and $8/9$ at $\lambda = 0.1$. Different values of N_h, M, and $N_{\rm phmax}$ were used to ensure that error bars, where not specified, are smaller than the sizes of the symbols.

triangles in Fig. 4(a), with details given in the figure caption. In the regime $\lambda \leqslant 0.1$, presented in Fig. 4(a), $\bar{j}$ decreases with increasing F for $F \gtrsim 0.1$. Our method does not yield steady-state results in the regime $F \lesssim 0.1$ due to large Stark localization length $L_S = 4t_0/F$. Since $\bar{j} = 0$ for $F = 0$ as well as in the opposite limit when $F \to \infty$, there must exist a global maximum value $\bar{j}_{\max}$ that depends on λ. For $\lambda = 0.1$, $\bar{j}_{\max} \sim 0.82$, while for $\lambda < 0.1$, $\bar{j}_{\max}$ is reached somewhere in the interval $0 < F < 0.1$, not accessible by the present numerical method. Choosing rational or even irrational values of ω_0/F leads to a decrease of $\bar{j}$ that nevertheless remains nonzero even in the latter case. A sweep over continuous values of F would lead to spikes in $\bar{j}$ located at integer values of ω_0/F, which is consistent with observations in previous works.[7–9,62]

To gain further insight into the decrease of $\bar{j}$ with F, we plot in Fig. 4(b) $\bar{j}/\sqrt{\lambda}$ versus $1/\sqrt{F}$ and realize that curves approximately collapse onto a straight line. The revealed scaling with $1/\sqrt{F}$ is a clear signature that we are dealing with a coherent propagation between Stark states with identical total energy that are spaced by $K = \omega_0/F$. This is in contrast to the assumption of an incoherent hopping between localized states,[7,8] which would predict a dependence $j \propto 1/F$. In turn, our derivation, as presented in the Appendix, leads for integer $K > 1$ as well as for $\omega_0 < W = 4t_0$ to a scaling of the maximum steady current

$$j_0 = \alpha \sqrt{\frac{\lambda \omega_0^3}{F}}. \tag{10}$$

While j_0 cannot be directly compared to the average current $\bar{j}$, the functional dependence on λ and F is in good agreement with scaling in Fig. 4(b) that leads to $\alpha \sim 0.89$ (the fit is represented by a dashed line). The expression in Eq. (10) is valid in the small λ and large F regime (however, $F < \omega_0$) where $\bar{j}$ decreases due to decreasing overlap between Stark states.

The scaling breaks down when, with decreasing F, $\bar{j}$ approaches the maximum $\bar{j}_{\max}$. In Fig. 4(c), we present results for larger $\lambda \in [0.2,2.0]$, which enables us to observe the evolution of $\bar{j}$ versus F as the system evolves from the weak EP coupling ($\lambda < 1$) toward the strong EP coupling ($\lambda > 1$) regime. With increasing λ, the position of $\bar{j}_{\max}$ shifts toward larger values of F while it decreases in its magnitude. The main difference between the weak and strong EP coupling regime emerges due to increasing energy gap Δ in the polaron excitation spectrum[56–58] that for $\lambda \gg 1$ approaches $\Delta \sim \omega_0$. Due to large Δ at large $\lambda > 1$, $\bar{j}$ remains zero until $F \sim F_{\text{th}}$.

We summarize the overview of numerical results with a diagram describing different regimes characterized by distinct short-time behaviors (after switching on F), presented in Fig. 4(d). We distinguish four different regimes: (i) The regime of damped free-particle BO's (DBO's) for small values of g. (ii) The almost critically damped (CD) regime, where steady-state current is reached in a time shorter than or of the order of t_B, and the oscillations in the current are still visible, however $j(t) > 0$ for any $t > 0$. (iii) The polaron BO regime (PBO), where the system evolves nearly adiabatically. The polaron Bloch oscillates within the polaron band and damping is exponentially small (numerically undetectable). In PBO's, the average current remains zero and total energy remains periodic within numerical accuracy and up to the largest measured time $t \leqslant 20t_B$. (iv) The damped polaron BO regime (DPBO), where remnants of PBO's are seen in $j(t)$ while there exists a measurable average current $\bar{j} > 0$ within $t \leqslant 20t_B$.

IV. CONCLUSIONS

In summary, we list our main results. Using a time-dependent Lanczos method, we have followed the time evolution of the polaron from its ground state toward the steady state after the electric field has been switched on. Different sizes of VHS have been used to ensure that the presented results are valid in the thermodynamic limit. Steady-state conditions have been reached at intermediate to high electric fields, and the current versus voltage characteristics have been plotted for different regimes of EP couplings. By calculating the electron-phonon correlation function representing the time evolution of the polaron, we show that the absorbed energy in the steady state is deposited as an increasing number of phonon excitations arranged as a growing tail behind the moving polaron.

The damped BO's can be observed in the extremely weak EP coupling limit. In the former case, the period of BO's $t_B = 2\pi/F$ should be less than the relaxation time t_0/g^2 related with the emission of phonons. A large gap in the spectrum in the strong-coupling regime is responsible for the observation of nearly perfect BO's arising from the polaron motion within the polaron band. The breakdown of this quasiadiabatic regime qualitatively resembles the Landau-Zener transition from the polaron band to higher excited states. An analytical estimate for the steady-state current on the electric field and the EP coupling constant at large fields is proposed and numerically tested. The unusual steady-state current versus electric-field dependence, $\bar{j} \propto \sqrt{\lambda/F}$, valid at large F and small λ, reflects the significance of coherent processes for a proper description of polaron motion. In contrast, approaches calculating the steady-state current relying on probabilities for transitions between neighboring Wannier-Stark states, mediated by the EP coupling, yield $\bar{j} \propto \lambda/F$.[7,8]

ACKNOWLEDGMENTS

We acknowledge stimulating discussions with C.D. Batista and financial support of the SRA under Grant No. P1-0044. J.B. and L.V. acknowledge financial support of the REIMEI project, JAEA, Japan.

APPENDIX: COHERENT PROPAGATION BETWEEN STARK STATES

To analyze the propagation of the polaron, an alternative approach to driven the Hamiltonian, Eq. (1), is to study eigenstates in a constant external electric field, i.e., the electron Hamiltonian is written as

$$H_e = -t_0 \sum_i (c_{i+1}^\dagger c_i + \text{H.c.}) - F \sum_i i n_i. \tag{A1}$$

Since eigenstates of H_e are localized Stark states, we perform the transformation to a new orthogonal basis,

$$\alpha_l = \sum_i w_{i-l} c_i, \tag{A2}$$

where wave functions w_j (being real) are localized in the interval $-L_S/2 < j < L_S/2$ with $L_s \sim 4t_0/F$, and eigenenergies $\epsilon_l = Fl + \epsilon_0$. To keep constant energy, the particle can propagate along the chain only by emitting (absorbing) phonons. The novel unperturbed term

$$H_0 = \sum_l \epsilon_l \alpha_l^\dagger \alpha_l + \omega_0 \sum_i a_i^\dagger a_i \tag{A3}$$

connects the average displacement in the Stark basis $\Delta\epsilon_l = F\Delta l$ to phonon generation $\omega_0 \Delta N_{\rm ph}$.

In the following, we consider only the simple commensurate case in which $\omega_0/F = K$ is an integer ($K > 1$, i.e., $F < \omega_0$), where electrons can perform coherent hopping between Stark states with $\Delta l = K$ keeping E_0 constant by emitting (or absorbing) a single phonon via the coupling term $H' = g\sum_i n_i(a_i^\dagger + a_i)$. Also, by restricting phonon frequencies to $\omega_0 < W = 4t_0$, we remain in the regime $K < L_S$. We now construct the basis of possible coherent states having the same $E_0 \sim 0$ starting with a bare electron state at $l = 0$ and generating novel states by application of H',

$$\begin{aligned} |\psi_0\rangle &= \alpha_0^\dagger |0\rangle, \\ \left|\psi_1^{j_1}\right\rangle &= \alpha_K^\dagger a_{j_1}^\dagger |0\rangle, \ldots, \\ \left|\psi_m^{j_1 j_2, \ldots, j_m}\right\rangle &= \alpha_{mK}^\dagger a_{j_1}^\dagger a_{j_1}^\dagger \cdots a_{j_m}^\dagger |0\rangle, \end{aligned} \tag{A4}$$

whereby j_m denote the location of phonons. The matrix elements between subsequent states can be evaluated explicitly by neglecting multiple occupations of sites (being rare for $K \gg 1$), i.e., $j_1 \neq j_2 \ldots$ or equivalently simplifying the boson factor for multiply occupied sites, i.e.,

$$\begin{aligned} &\left\langle \psi_m^{j_1,\ldots,j_{m-1}j_m} \middle| H' \middle| \psi_{m-1}^{j_1,\ldots,j_{m-1}} \right\rangle \\ &\quad \sim g w_{j_m - mK} w_{j_m - (m-1)K} = T_{j_m}, \end{aligned} \tag{A5}$$

which depends within such an approximation only on $\tilde{j}_m = j_m - mK$. We search now for the eigenstates in such a restricted space in the form

$$\begin{aligned} |\Psi\rangle = b_0|\psi_0\rangle + \sum_{j_1} b_1^{j_1} \left|\psi_1^{j_1}\right\rangle + \cdots \\ + \sum_{j_1, j_2, \ldots, j_m} b_m^{j_1, j_2, \ldots, j_m} \left|\psi_m^{j_1, j_2, \ldots, j_m}\right\rangle \cdots, \end{aligned} \tag{A6}$$

where the energies $\tilde{E}$ are obtained solving the system

$$\begin{aligned} \tilde{E} b_0 &= \sum_{j_1} T_{j_1} b_1^{j_1}, \\ \tilde{E} b_1^{j_1} &= T_{j_1} b_0 + \sum_{j_2} T_{j_2} b_2^{j_1 j_2}, \\ \tilde{E} b_m^{j_1,\ldots,j_m} &= T_{j_m} b_{m-1}^{j_1,\ldots,j_{m-1}} + \sum_{j_{m+1}} T_{j_{m+1}} b_{m+1}^{j_1,\ldots,j_{m+1}}. \end{aligned} \tag{A7}$$

By inserting the solutions of the Stark problem into Eq. (A5), the branching system, Eq. (A7), can be solved quite generally. Here, we are interested only in a qualitative behavior, hence we use the simplification

$$T_j \sim \frac{g}{L_S}(-1)^{r_j}, \quad -L_S/2 + K < j < L_S/2, \tag{A8}$$

and $T_j = 0$ elsewhere, where the phase $(-1)^{r_j}$ emerges from fast varying Stark functions w_j in Eq. (A5).

Solutions of Eqs. (A7) and (A8) can be found by an ansatz,

$$b_{m+1}^{j_1,\ldots,j_{m+1}} \sim e^{-ipK} \frac{1}{\sqrt{\tilde{L}_S}} (-1)^{r_{j_{m+1}}} b_m^{j_1,\ldots,j_m}, \tag{A9}$$

where $\tilde{L}_S = L_S - K$. The corresponding eigenenergies are

$$\tilde{E} = \tilde{E}_p = \frac{2g}{L_s}\sqrt{\tilde{L}_S}\cos(pK), \tag{A10}$$

which leads to group velocities in the tight-binding form $v_p \propto v_p = v_0 \sin(pK)$ with the maximum

$$v_0 \simeq \frac{2gK}{L_S}\sqrt{\tilde{L}_S} \sim \frac{2gK}{\sqrt{L_S}} = \frac{g\omega_0}{\sqrt{t_0 F}}. \tag{A11}$$

The derivation can be made more rigorous taking into account the actual Stark wave functions w_j and matrix elements Eq. (A5). Still, it is not expected to change qualitatively the scaling of coherent group velocities v_p with the maximum v_0, Eq. (A11). It should be remembered, however, that we did not yet match the actual solution Eq. (A10) with the boundary condition, as determined, e.g., with the first equation in the system Eq. (A7). In any case, it is expected that an eigenstate of a stationary Hamiltonian, as in Eq. (A1), cannot possess a finite steady current (the solution being a superposition of $\pm p$ eigenstates). On the other hand, the driven system and the time-dependent model, Eq. (1), clearly can generate the current $j(t)$ and in this sense induce solutions with the steady current $\bar{j} \propto j_0 = v_0$ following Eq. (A11). Evidently, a more rigorous relation between the eigenstates of the stationary case and the driven problem is still desired.

[1] T. Oka, R. Arita, and H. Aoki, Phys. Rev. Lett. **91**, 066406 (2003).
[2] H. Fehske, J. Schleede, G. Schubert, G. Wellein, V. S. Filinov, and A. R. Bishop, Phys. Lett. A **373**, 2182 (2007).
[3] S. R. White and A. E. Feiguin, Phys. Rev. Lett. **93**, 076401 (2004).
[4] J. K. Freericks, V. M. Turkowski, and V. Zlatić, Phys. Rev. Lett. **97**, 266408 (2006).
[5] K. K. Thornber and R. P. Feynman, Phys. Rev. B **1**, 4099 (1970).
[6] F. S. Khan, J. H. Davies, and J. W. Wilkins, Phys. Rev. B **36**, 2578 (1987).
[7] D. Emin and C. F. Hart, Phys. Rev. B **36**, 2530 (1987).
[8] S. Rott, N. Linder, and G. H. Döhler, Phys. Rev. B **65**, 195301 (2002).
[9] J. Bonča and S. A. Trugman, Phys. Rev. Lett. **79**, 4874 (1997).
[10] A. Johansson and S. Stafström, Phys. Rev. Lett. **86**, 3602 (2001).

[11] D. M. Basko and E. M. Conwell, Phys. Rev. Lett. **88**, 056401 (2002).
[12] A. A. Johansson and S. Stafström, Phys. Rev. B **69**, 235205 (2004).
[13] X. Liu, K. Gao, J. Fu, Y. Li, J. Wei, and S. Xie, Phys. Rev. B **74**, 172301 (2006).
[14] Y. Li, X. J. Liu, J. Y. Fu, D. S. Liu, S. J. Xie, and L. M. Mei, Phys. Rev. B **74**, 184303 (2006).
[15] Y. Qui and L.-P. Zhu, J. Chem. Phys. **131**, 134903 (2009).
[16] M. Peyrard and A. R. Bishop, Phys. Rev. Lett. **62**, 2755 (1989).
[17] S. Komineas, G. Kalosakas, and A. R. Bishop, Phys. Rev. E **65**, 061905 (2002).
[18] P. Maniadis, G. Kalosakas, K. O. Rasmussen, and A. R. Bishop, Phys. Rev. B **68**, 174304 (2003).
[19] P. Maniadis, G. Kalosakas, K. O. Rasmussen, and A. R. Bishop, Phys. Rev. E **72**, 021912 (2005).
[20] J. A. Berashevich, V. Apalkov, and T. Chakraborty, J. Phys. Condens. Matter **20**, 075104 (2008).
[21] E. Diaz, R. P. A. Lima, and F. Dominguez-Adame, Phys. Rev. B **78**, 134303 (2008).
[22] E. Diaz and F. Dominguez-Adame, Chem. Phys. **365**, 24 (2009).
[23] C.-M. Chang, A. H. Castro Neto, and A. R. Bishop, Chem. Phys. **303**, 189 (2004).
[24] H. Yamada, E. B. Starikov, and D. Hennig, Eur. Phys. J. B **185**, 185 (2007).
[25] E. Macia, Phys. Rev. B **76**, 245123 (2007).
[26] J. Feldmann, K. Leo, J. Shah, D. A. B. Miller, J. E. Cunningham, T. Meier, G. von Plessen, A. Schulze, P. Thomas, and S. Schmitt-Rink, Phys. Rev. B **46**, 7252 (1992).
[27] K. Leo, P. Harig Bolivar, F. Brüggemann, R. Schwedler, and K. Köhler, Solid State Commun. **84**, 943 (1992).
[28] C. Waschke, H. G. Roskos, R. Schwedler, K. Leo, H. Kurz, and K. Köhler, Phys. Rev. Lett. **70**, 3319 (1993).
[29] E. E. Mendez, F. Agullo-Rueda, and J. M. Hong, Phys. Rev. Lett. **60**, 2426 (1988).
[30] P. Voisin, J. Bleuse, C. Bouche, S. Gaillard, C. Alibert, and A. Regreny, Phys. Rev. Lett. **61**, 1639 (1988).
[31] M. Ben Dahan, E. Peik, J. Reichel, Y. Castin, and C. Salomon, Phys. Rev. Lett. **76**, 4508 (1996).
[32] S. R. Wilkinson, C. F. Bharucha, K. W. Madison, Q. Niu, and M. G. Raizen, Phys. Rev. Lett. **76**, 4512 (1996).
[33] Q. Niu, X.-G. Zhao, G. A. Georgakis, and M. G. Raizen, Phys. Rev. Lett. **76**, 4504 (1996).
[34] B. P. Anderson and M. A. Kasevich, Science **282**, 1686 (1998).
[35] A. R. Kolovsky, E. A. Gomez, and H. J. Korsch, Phys. Rev. A **81**, 025603 (2010).
[36] O. Morsch, J. H. Müller, M. Cristiani, D. Ciampini, and E. Arimondo, Phys. Rev. Lett. **87**, 140402 (2001).
[37] G. Ferrari, N. Poli, F. Sorrentino, and G. M. Tino, Phys. Rev. Lett. **97**, 060402 (2006).
[38] A. Buchleitner and A. R. Kolovsky, Phys. Rev. Lett. **91**, 253002 (2003).
[39] W. S. Dias, E. M. Nascimento, M. L. Lyra, and F. A. B. F. de Moura, Phys. Rev. B **76**, 155124 (2007).
[40] R. Khomeriki, D. O. Krimer, M. Haque, and S. Flach, Phys. Rev. A **81**, 065601 (2010).
[41] F. Dominguez-Adame, V. A. Malyshev, F. A. B. F. de Moura, and M. L. Lyra, Phys. Rev. Lett. **91**, 197402 (2003).
[42] J. Bonča, S. A. Trugman, and I. Batistić, Phys. Rev. B **60**, 1633 (1999).
[43] J. Bonča, S. Maekawa, T. Tohyama, and P. Prelovšek, Phys. Rev. B **77**, 054519 (2008).
[44] G. Wellein and H. Fehske, Phys. Rev. B **56**, 4513 (1997).
[45] S. Ciuchi, F. de Pasquale, S. Fratini, and D. Feinberg, Phys. Rev. B **56**, 4494 (1997).
[46] E. Jeckelmann and S. R. White, Phys. Rev. B **57**, 6376 (1998).
[47] A. W. Romero, D. W. Brown, and K. Lindenberg, J. Chem. Phys. **109**, 6540 (1998).
[48] A. S. Alexandrov, *Polarons in Advanced Materials, Springer Series in Material Sciences*, Vol. 103 (Springer, Dordrecht, 2007).
[49] M. Berciu and G. L. Goodvin, Phys. Rev. B **76**, 165109 (2007).
[50] O. S. Barišić and S. Barišić, Eur. Phys. J. B **64**, 1 (2008).
[51] Z. Li, D. Baillie, C. Blois, and F. Marsiglio, Phys. Rev. B **81**, 115114 (2010).
[52] A. Alvermann, H. Fehske, and S. A. Trugman, Phys. Rev. B **81**, 165113 (2010).
[53] M. Zoli, Adv. Condens. Matter Phys. **2010**, 815917 (2010).
[54] P. T. Jun and J. C. Light, J. Chem. Phys. **85**, 5870 (1986).
[55] M. Mierzejewski and P. Prelovšek, Phys. Rev. Lett. **105**, 186405 (2010).
[56] O. S. Barišić, Phys. Rev. B **69**, 064302 (2004).
[57] O. S. Barišić, Phys. Rev. B **73**, 214304 (2006).
[58] L. Vidmar, J. Bonča, and S. A. Trugman, Phys. Rev. B **82**, 104304 (2010).
[59] L. Landau, Phys. Z. Sowjetunion **2**, 46 (1932).
[60] C. Zener, Proc. R. Soc. London, Ser. A **137**, 696 (1932).
[61] T. Oka and H. Aoki, Phys. Rev. Lett. **95**, 137601 (2005).
[62] W. Zhang, A. O. Govorov, and S. E. Ulloa, Phys. Rev. B **66**, 134302 (2002).